Nuclear-mitochondrial crosstalk in the heart during diabetes mellitus – the impact on RNA in mitochondrial subpopulations

Quincy A. Hathaway, Danielle L. Shepherd, Andrya J. Durr, and John M. Hollander

West Virginia University, Morgantown, WV

Abstract

The cellular milieu, with changing substrate utilization, ROS, inflammation, and other factors, influences the function of the mitochondrion, which plays a vital role in bioenergetics. How the mitochondrion functions is affected both by the import of nuclear-encoded mitochondrial proteins and by regulation of RNA transcripts within the mitochondrion. We have previously shown during diabetes mellitus, that pathways involving protein (HSPA9) and small RNA (PNPase) import are directly impacted. The implications of epigenetic control of the genome, which is shown to be globally altered in the diabetic heart, is relatively unexplored in regards to mitochondrial health and function. Type 2 Diabetic and non-diabetic human right atrial tissue and db/db mouse whole heart were used for evaluation of epigenetic modifications to nuclear-encoded mitochondrial proteins involved in protein and RNA import into the mitochondrion, HSPA9 and PNPT1, respectively. Also, analysis of human atrial mitochondrial RNA was examined. The promoter region of HSPA9 and PNPT1 were processed for histone activation/repression (H3K4me3 and H3K27me3, respectively) and DNA methylation. Chromatin-immunoprecipitation qPCR evaluated differentially bound regions of H3K4me3 and H3K27me3. Bisulfite treatment, methylation PCR, and cloning were used to measure methylation status of CpG islands. Small RNAs were sequenced through NextGen sequencing for mitochondrial subpopulations, subsarcolemmal (SSM) and interfibrillar (IFM). During the diabetic pathology, HSPA9 was shown to have increased H3K27me3 association in human and mouse ($P \leq 0.05$), while PNPT1 exhibited significantly lower H3K27me3 ($P \leq 0.05$) and higher H3K4me3 ($P \leq 0.05$) association in human and mouse. Neither gene had differential methylation patterns during type 2 diabetes mellitus. In type 2 diabetes mellitus, all human mitochondrial transcribed RNA transcripts had a significant decrease in expression in the SSM ($P_{adj} \leq 0.05$), while no changes in the IFM were observed. Our results suggest that during type 2 diabetes mellitus, nuclear-encoded proteins that comprise the mitochondrial proteome and are involved in protein and RNA import can be epigenetically altered. Mitochondrial subpopulations also differentially express RNA during diabetic insult, with the SSM being more detrimentally impacted. Epigenetic alterations, and changes in RNA, reveal how environmental changes to the nuclear genome could shape mitochondrial structure and function.

Introduction

- Cardiovascular diseases remain the primary factors influencing mortality worldwide.
- The development of diabetes mellitus doubles an individuals chances of an adverse, cardiac event, with co-morbidities such as hypertension quadrupling the risk.
- In 2015, more than 30 million people were diagnosed with diabetes mellitus in the United States alone, comprising almost 10% of the total population.

Figure 1

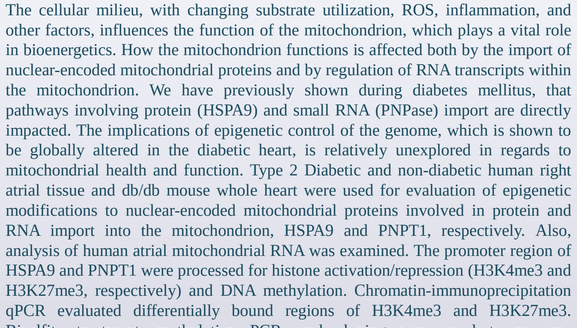

Figure 1: Mitochondrial protein and RNA import constituents. Tom40, Tim 23, mtHsp70, and other proteins are known to comprise the protein import pathways of the mitochondrion. Import of non-coding RNA (ncRNA) is suggested to occur through a pore in the mitochondrion (VDAC) or through facilitated transport by PNPase and/or Ago2. The maintenance of both the mitochondrial protein and ncRNA import are important in shaping mitochondrial structure, function, and cellular homeostasis.

Figure 2

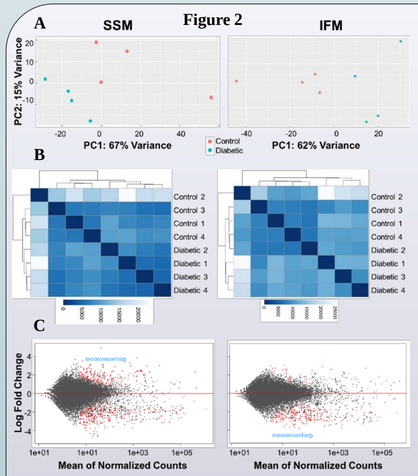

Figure 2: Sample metrics for SSM and IFM of human right atrial mitochondria, differences expressed between diabetic and non-diabetic. **(A)** Principle Component Analysis (PCA) for sample distribution, revealing both intra- and inter sample variance. **(B)** Raw count matricies for sample-to-sample distribution implementing the PoiClaClu package in R. **(C)** The MA-plot reveals the differentially expressed genes (red, $P_{adj} \leq 0.05$) in comparison to genes with non-significant change between groups (grey). The most differentially expressed gene is circled in blue.

Figure 3

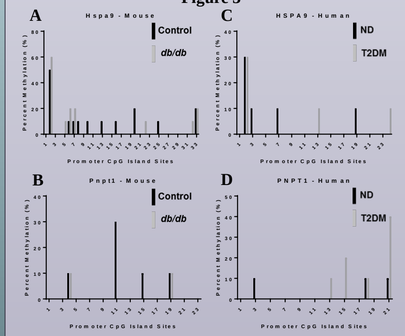

Figure 3: CpG island methylation for HSPA9 and Hspa9**.** CpG island methylation in the promotor region of **(A)** Hspa9 and **(B)** Pnpt1 in control (black, n = 6) versus *db/db* (grey, n = 6) mice whole heart. CpG island methylation in the promotor region of **(C)** HSPA9 and **(D)** PNPT1 in non-diabetic (black, n = 6) versus type 2 diabetic (grey, n = 6) human right atrial tissue. For both human and mouse CpG methylation, 10 clones were selected from each group. ND = non-diabetic, T2DM = type 2 diabetes mellitus.

Materials and Methods

CpG island DNA methylation: Mouse cardiac tissue was lysed and DNA isolated using spin column purification. Primers were designed to span a portion of the CpG island located at the promoter region of the HSPA9 and Hspa9 genes. Platinum™ Taq DNA Polymerase was used to amplify CpG islands. PCR products were run on a 2% agarose gel and bands were excised and purified. Purified DNA was incorporated into a TOPO (topoisomerase) plasmid and transfected into DH5α E. coli cells. Plasmids were isolated and sent to the West Virginia University Genomics Core Facility for Sanger sequencing.

Histone modifications: ChIP (chromatin immunoprecipitation) was performed on human atrial appendage and mouse cardiac tissue. Briefly, tissue was homogenized and transiently crosslinked with 37% formaldehyde. 1M glycine stopped crosslinking and chromatin shearing was conducted. Chromatin marks studied in the experiment were histone 3 lysine 4 tri-methylation (H3K4me3) and histone 3 lysine 27 tri-methylation (H3K27me3). The DNA recovered from ChIP was used for qPCR.

Histone Methyltransferase Activity: Global H3K27me3 levels were assessed using the EpiQuik™ Global Tri-Methyl Histone H3-K27 Quantification Kit (Colorimetric), per manufacturer's instructions. Briefly, nuclear fractions were isolated using differential centrifugation. 2 µg of nuclear fractions were run in triplicate for each sample, prepared on anti-H3K27me3 antibody coated strip wells. Colorimetric analyses was performed using the Flexstation 3 Luminometer.

Quantitative PCR: RNA was isolated from human atrial appendage and cardiac mouse tissue using the miRNeasy® Mini Kit, per manufacturer's instructions. RNA was converted to cDNA using a First-strand cDNA Synthesis kit for miRNA, per manufacturer's instructions. The mRNA of transcripts within the PCR2 complex were normalized to GAPDH. Chromatin-immunoprecipitation (ChIP)-qPCR was normalized to the input control for each sample. Experiments were performed on the Applied Biosystems 7900HT Fast Real-Time PCR system, using. Quantification was achieved using the $2^{-\Delta\Delta CT}$ method.

Mitochondrial Subpopulations: Subsarcolemmal mitochondria (SSM) and interfibrillar mitochondria (IFM) subpopulations were isolated as previously described (Palmer et al. 1977) with minor modifications by our laboratory (Dabkowski et al. 2010; Baseler et al. 2011, 2013; Croston et al. 2013; Thapa et al. 2015). Mitochondrial pellets were resuspended in KME buffer (100mM KCl, 50mM MOPS and 0.5mM EGTA pH 7.4) and utilized for all analyses.

Cross-linking Immunoprecipitation (CLIP): CLIP was performed as previously described (Jagannathan et al. 2015), with some modifications. Anti-Ago2 and anti-PNPASE were used for protein pulldown. After RNA 3'-end biotinylation labeling, samples were loaded into SDS-PAGE. The membrane above the protein of interest was excised, RNA isolated, samples pooled (n = 5 per group) and submitted for Next-Generation Sequencing

RNA Preparation for Next-Generation Sequencing: RNA was purified either from human right atrial appendage total isolated mitochondria or human right atrial appendage and animal whole heart protein-RNA pulldowns, using the miRNeasy Mini Kit. Library preparation was performed using NEXTflex® Small RNA Sequencing Kit v3 for total mitochondria and TruSeq smallRNA Library Prep for protein-RNA pulldowns. Each sample was run across two lanes of the Illumina Hi-Seq in Rapid Run mode for total mitochondrial miRNA and on one lane of the MiSeq for pooled CLIPed samples.

Bioinformatics: Generated Fastq files were further processed through HiISAT2 (total mitochondrial miRNA) and Bowtie (anti-PNPASE RNA). Resulting BAM files were aligned to the reference genomes for human (Homo_sapiens.GRCh38.91.gtf.gz) or mouse (Mus_musculus.GRCm38.91.gtf.gz) were applicable. The R environment was used to asses sample distribution and differential gene expression through DESeq2.

Statistics: All measures of significance between the control and diabetic groups for the sequencing data are presented as adjusted *P*-values. Adjusted *P*-values are a composition of standard, unadjusted P-values and the stringency of the False Discovery Rate (FDR). Differential expression analysis through DESeq2 implements the Wald Test, using multiple testing against the null hypothesis that P-values are uniformly distributed across a data set, known as the Benjamini-Hochberg procedure. The FDR for was set at 0.05.

Results

Figure 4

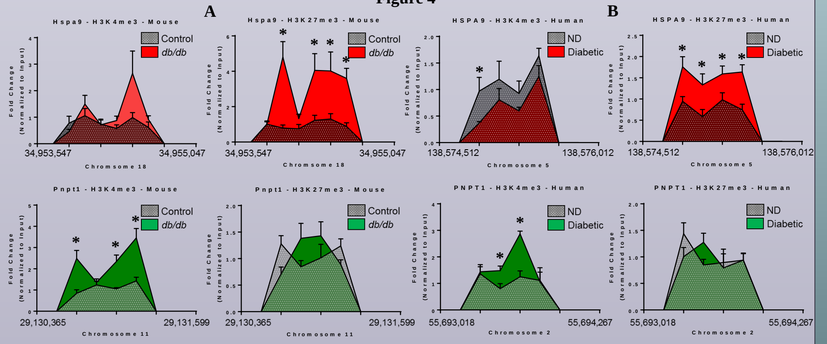

Figure 4: Changes in histone methylation dynamics for Hspa9, HSPA9, Pnpt1, and PNPT1. Histone peaks were assessed at the mouse **(A)** Hspa9 and Pnpt1 promoter for H3K4me3 (n = 6) and H3K27me3 (n = 6) and at the human **(B)** HSPA9 and PNPT1 promoter for H3K4me3 (n = 6) and H3K27me3 (n = 6). Values are expressed as means ± SEM. **P* ≤ 0.05 for control vs. diabetes mellitus. ChIP-qPCR samples were normalized to their respective input control. H3K4me3 = histone 3 lysine 4 tri-methylation, H3K27me3 = histone 3 lysine 27 tri-methylation, ND = non-diabetic, T2DM = type 2 diabetes mellitus.

Figure 5

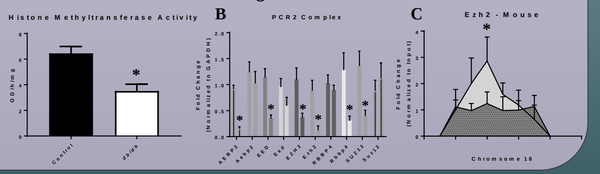

Figure 5. Mechanisms affecting HSPA9 Epigenetics. **(A)** global histone methyltransferase activity for H3K27me3 was assessed in control (n = 5) and db/db (n = 5) mouse whole heart. Further, **(B)** constituents of the PCR2 complex were measured through qPCR in both human (ND and T2DM, n = 5) and mouse (control and *db/db*, n = 5) cardiac tissue. At the Hspa9 promoter loci, **(C)** ChIP pulldown and qPCR was performed for Ezh2. Values are expressed as means ± SEM. **P* ≤ 0.05 for control vs. diabetes mellitus. ChIP-qPCR samples were normalized to respective input control. GAPDH was used to normalize PCR2 components. H3K27me3 = histone 3 lysine 27 tri-methylation, PCR2 = Polycomb Repressive Complex 2.

Results

Figure 6

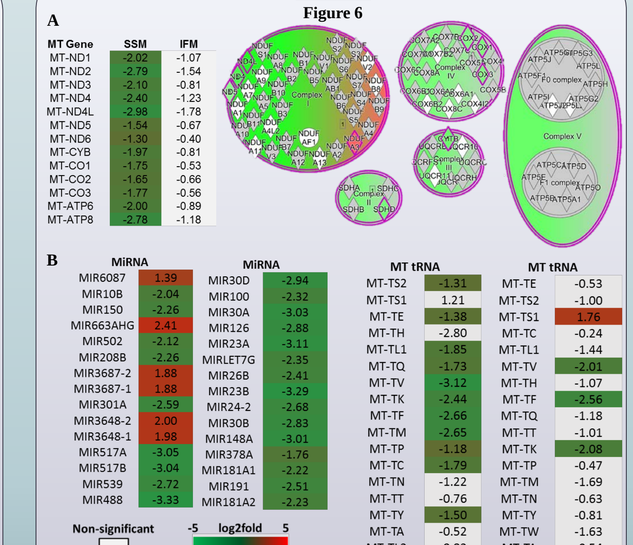

Figure 6: Transcriptomic changes in the SSM and IFM between diabetic and non-diabetic human right atrial mitochondria. **(A)** Heatmap depicting changes in the expression of mitochondrial transcribed genes in the SSM and IFM. Ingenuity Pathway Analysis (IPA) depiction of mitochondrial electron transport chain complexes and suggested changes to proteins. Green = significant decrease, red = significant increase in expression ($P_{adj} \leq 0.05$). **(B)** The top miRNAs and mitochondrial transcribed tRNAs differentially expressed following diabetic insult.

Conclusions

Figure 7

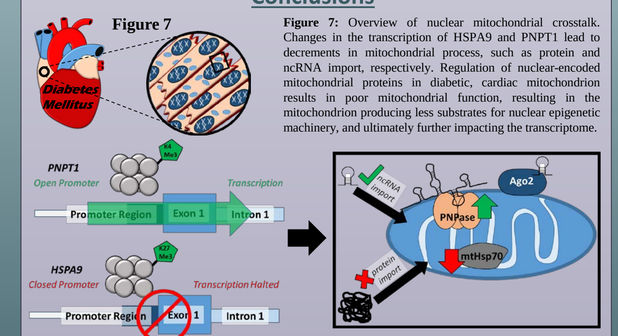

Figure 7: Overview of nuclear mitochondrial crosstalk. Changes in the transcription of HSPA9 and PNPT1 lead to decrements in mitochondrial process, such as protein and ncRNA import, respectively. Regulation of nuclear-encoded mitochondrial proteins in diabetic, cardiac mitochondrion results in poor mitochondrial function, resulting in the mitochondrion producing less substrates for nuclear epigenetic machinery, and ultimately further impacting the transcriptome.

Grants

This work was supported by the National Institutes of Health from the National Heart, Lung and Blood Institute grant HL128485 and the WVU CTSI grant U54GM104942 awarded to JMH. This work was supported by an American Heart Association Predoctoral Fellowship grant AHA 14PRE19890020 awarded to DLS This work was supported by a National Science Foundation IGERT: Research and Education in Nanotoxicology at West Virginia University Fellowship grant 1144676 awarded to QAH. This work was supported by an American Heart Association Predoctoral Fellowship (AHA 17PRE33660333) awarded to QAH. Ingenuity Pathway Analyses were supported by WV INBRE Grant P20 GM103434.